Electronic Supplementary Information (ESI)

Julolidine Functionalized Benzimidazoline n-Dopant: Optimizing Molecular Doping in Fullerene Derivatives by Modulating Miscibility

Chenglong Li,[a] Wei Wang,[a] Chun Zhan,*[a] Qisheng Zhou,[a] Defu Dong,[a] Shengqiang Xiao*[ab]

[a] State Key Laboratory of Advanced Technology for Materials Synthesis and Processing, Wuhan University of Technology, Wuhan, 430070, P. R. China.

[b] Hubei Key Laboratory of Fuel Cell, Wuhan 430070, China.

*Corresponding author, E-mails: zhanc@whut.edu.cn (C.Z.), shengqiang@whut.edu.cn (S.X.)

The list of the content：

1. Materials

Chemicals were obtained from Sinopharm Chemical Reagent and Energy Chemical and used as received unless stated. *N,N′*-Dimethyl-*o*-phenylenediamine[1], PTEG-1 and PTEG-2[2] were synthesized as previously reported. $PC_{61}BM$ and 9-julolidinecarboxaldehyde were purchased from *Solenne* and *Energy Chemical*, respectively.

2. Measurements and Instruments

^{1}H NMR and ^{13}C NMR spectra were performed on a Bruker Advance III-HD-500MHz at 298K in $CDCl_3$ with tetramethylsilane (TMS) as internal standard. The chemical shifts (δ) are reported in parts per million (ppm). NMR spectra for **JLBI-H** are shown in Fig. S1and S2. The mass spectroscopy measurement (Fig. S3) was performed on a SHIMADZU GCMS-QP2020 spectrometer.

Thermogravimetric analysis (TGA) were performed on a NETZSCH-STA449C from 30 to 500 ^{o}C under N_2 with a heating rate of 10 ^{o}C min^{-1}. Differential scanning calorimetry (DSC) measurement of the pristine dopant was performed from 30 to 200 ^{o}C under N_2 with a heating rate of 10 ^{o}C min^{-1} on PerkinElmer DSC-8500 instrument. The samples were dried in a vacuum oven overnight prior to the TGA and DSC measurements.

The cyclic voltammetry (CV) experiment of **JLBI-H** were performed in solution on a CHI 605E analyzer at room temperature. The measurement was carried out in 0.1 M tetrabutylammonium hexafluorophosphate (Bu_4NPF_6) in deaerated anhydrous acetonitrile

with a conventional three-electrode configuration employing a platinum wire as the counter electrode, a platinum disk electrode as the working electrode, and ferrocene as the internal reference at a scan rate of 80 mV s^{-1}. **JLBI-H** was added into the electrolyte solution with a concentration of 1.0 mM.

The electronic structures of **JLBI-H** and **JLBI$^\cdot$** were calculated at the B3LYP/6-311++g(d,p) level of theory using the Gaussian16 program package.[3] The method in combination with the polarizable continuum model (PCM) was used for the optimizations of geometric structures and calculations of the total energies and the enthalpy changes in this work.[4] The highest occupied molecular orbital (HOMO), lowest unoccupied molecular orbital (LUMO) and singly occupied molecular orbital (SOMO) of the models were analyzed by using gaussian view.

UV−vis spectra were recorded on a SHIMADZU UV-1750 spectrophotometer in air at room temperature. The absorption of **JLBI-H** was recorded as in solution with a concentration of 1×10^{-5} M in dichloromethane (DCM). The thickness of the pure and **JLBI-H**-doped fullerene derivative films was around 100 ± 5 nm, which were measured with a Bruker DEKTAK-XT profilometry.

Atomic force microscopy (AFM) was performed with ScanAsyst mode on Bruker Dimension FastScan, using RTESPA-ScanAsyst-Air tips (Bruker, resonnant frequency 70 kHz, spring constant 0.4 N m^{-1}, tip radius 5 nm) for the measurements. We scanned all samples at a fixed scan rate of 1 Hz and 256 samples/line at a fix aspect ratio of 1. AFM

images (5 × 5 μm) were processed and analyzed in NanoScope Analysis 1.5 Software (Bruker, USA) to calculate roughness.

The grazing incident wide-angle X-ray scattering (GIWAXS) measurements were carried out with a Xeuss 3.0 SAXS/WAXS laboratory beamline using a Cu X-ray source (8.05 keV, 1.54 Å) and an Eiger2R 1M detector with an optimized incidence angle of 0.22°. All of the tested films were spin-coated on precleaned silicon substrates.

3. Fabrication and Characterization of Doped Samples

Glass substrates were ultrasonically cleaned with deionized water, acetone and isopropanol for 20 minutes in sequence, then dried by nitrogen gun and cleaned with a UV-Ozone cleaner for 10 minutes. The blend solutions of fullerene ($PC_{61}BM$, PTEG-1, PTEG-2, 10 mg mL^{-1} in chloroform) with dopants (**JLBI-H** or *N*-DMBI-H) were prepared by adding certain amount of dopant solution (10 mg mL^{-1} in chloroform) at varying dopant molar fractions to the individual fullerene derivative solutions under nitrogen atmosphere. The blend solutions of fullerene with dopant needs to be stirred for 20 minutes to ensure uniform blending of the dopant and the host. Subsequently, the mixture is spin-coated at various speed onto clean glass substrates to obtain films with varied thickness. The pristine fullerene films were prepared in the same way. The doping was then fully activated by annealing the above films in a N_2-filled glovebox (H_2O < 0.1 ppm, O_2 < 0.1 ppm).

Conductivity Measurement

Before electrical conductivity, 80 nm thick parallel strip Ag electrodes were deposited as the top contacts (channel length L = 8 mm and width w = 2 mm) at a pressure of 2×10^{-6} mbar through a shadow mask. The electrical conductivity (σ) and Seebeck coefficient (S) were measured under nitrogen atmosphere by a standard four-probe method on an apparatus (Cryoall CTA-3) for thermoelectrical measurements. The conductivity was calculated according to $\sigma = w/(RLd)$, where d and R are the thickness of the film after annealing and the resistance of test area, respectively.

Optimization of Doping Conditions

Presetting a relatively lower dopant fraction of 15 mol% and the thermal annealing temperature at 125 °C (close to the melting point of **JLBI-H**) for 1 h, the effect of film thickness on the electrical conductivity of **JLBI-H**-doped films was thus firstly probed as indicated in Fig. S9a. It is revealed that the electrical conductivity of the doped $PC_{61}BM$ films at room temperature is almost constant around 0.70 S cm^{-1} with thickness from 50 nm up to 150 nm. For the doped PTEG-1 films，the electrical conductivity increases slightly by increasing the film thickness from 1.86 S cm^{-1} in 50 nm film to 2.02 S cm^{-1} in 60 nm film. However, no significant change is observed when further increase the film thickness up to 165 nm. The conductivity of the doped PTEG-2 films increases from 0.44 S cm^{-1} to 0.87 S cm^{-1} as the film thickness increased from 35 nm to 100 nm and then slightly decreases to 0.57 S cm^{-1} in 130 nm film and 0.54 S cm^{-1} in 160 nm film. To eliminate the effect of different film thickness on the **JLBI-H** doped $PC_{61}BM$, PTEG-1 and PTEG-2

films, electrical property characterization was then carried out on the doped films all with 100 nm thickness by further optimizing the annealing temperature and duration. Presented in Fig. S9b,c and d are the exploration on the impact of thermal annealing temperature and annealing time on the conductivity of the 15 mol% **JLBI-H**-doped $PC_{61}BM$, PTEG-1 and PTEG-2 films. For the **JLBI-H**-doped $PC_{61}BM$ films, a longer annealing time (4 h) was required to reach the σ_{max} at 100 ^{o}C, while the σ_{max} (~ 0.65 S cm^{-1}) was achieved when annealed at 125 ^{o}C over 1 h. A higher annealing temperature (150 ^{o}C) led to an overall decrease in film conductivity. For doped PTEG-1 and PTEG-2 films, the same overall decrease in conductivity was observed as well when annealed at 150 ^{o}C. Similarly, it took longer to reach the σ_{max} at 100 ^{o}C (4-6 h), while only for 1 h at 125 ^{o}C with the σ_{max} of 2.04 and 0.87 S cm^{-1} for PTEG-1 and PTEG-2, respectively. Namely, annealing for about 1 h was found sufficient to allow for efficient doping at optimum annealing temperature of 125 ^{o}C.

Carrier Concentration and Electronics Mobility

The MIS device in this work have an architecture of indium-tin-oxide (ITO)/ion-gel insulator/fullerene derivative film/Al. We employed a mixture of poly(vinylidene fluoride-co-hexafluoropropylene) (PVDF-HFP) and 1-ethyl-3-methylimidazolium bis(trifluoromethylsulfony) imide ([EMIM][TFSI]) as the ion-gel insulator. The ion-gel solution was prepared by following the previously reported method, and then spin-coated onto clean patterned ITO substrate with thickness of 150-300 nm followed by annealing at

140 °C for 4 h. After spin-coating the active layer onto the insulating layer, 100 nm thick Al was deposited as the top electrode, with a testing area of 2×2 mm^2. The C_p-V characteristics of the MIS devices were conducted at a frequency of 10 Hz for AC bias. The carrier concentrations (n) of the semiconductor layers then can be calculated from the

C_p^{-2}-V characteristics by Mott-Schottky analysis: $n = \dfrac{2}{q\varepsilon_0\varepsilon_r\left(\dfrac{\partial C_p^{-2}}{\partial V}\right)}$, where ε_0 is the permittivity of free space, ε_r is the dielectric constant of the active layer, q is the elementary charge and C_p is the specific capacitance of the device.

Conventional bottom-gated top-contact OFET devices to acquire charge carrier mobility (μ_e), which were extracted from the saturation region of the transfer curves. Bottom-gate top-contact OFETs were fabricated on highly doped Si wafers with a 100 nm SiO$_2$ dielectric layer. The substrates were first cleaned with piranha solution (volume ratio: H$_2$SO$_4$:H$_2$O$_2$ = 7:3) for 20 minutes, followed by multiple ultrasonic cleaning with deionized water, and then baked in oven at 70 °C for 20 minutes. the cleaned and dried substrates were exposed to UV/ozone for 20 minutes in a UV/ozone cleaner. The blend solutions of fullerene with **JLBI-H** were spin-casted on the precleaned substrates under nitrogen atmosphere. Source and drain electrodes (channel length W = 2 mm and width L = 100 μm) were formed on top of the active layers by thermally evaporating Au (60 nm) through a shadow mask. The OFET properties were characterized using a Keithley 4200-SCS semiconductor parameter analyzer. The saturation mobility was calculated using the

following equation of $I_{DS} = (WC_i/2L)\mu(V_G - V_T)^2$, where C_i (11.5 nF cm^{-2}) is the unit area capacitance of the SiO$_2$ dielectric, I_{DS} refers to the drain current, V_G and V_T represent the gate voltage and the threshold voltage, respectively.

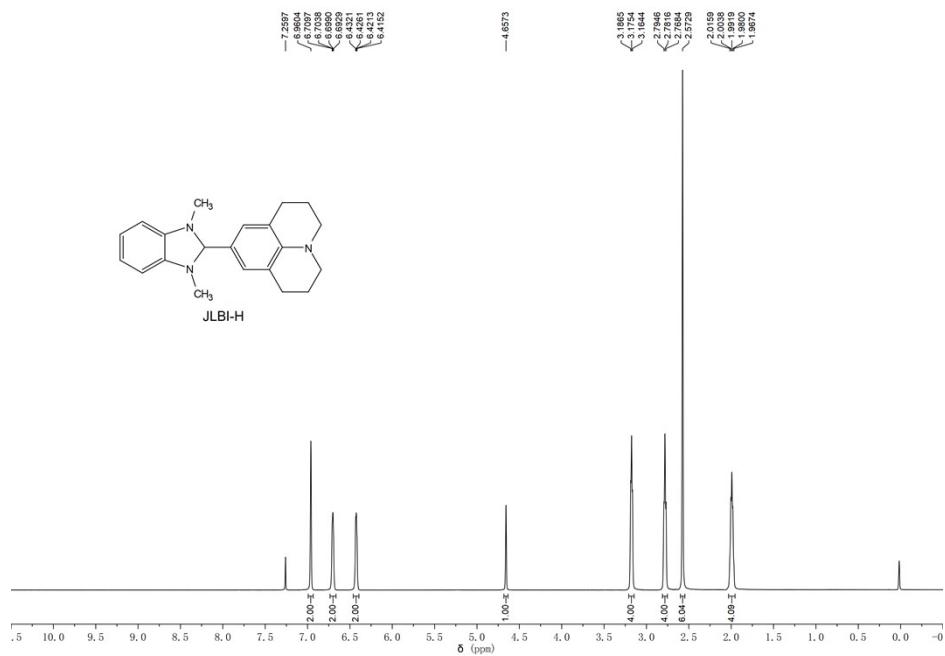## 4. The NMR Spectra and Mass Spectrum of JLBI-H
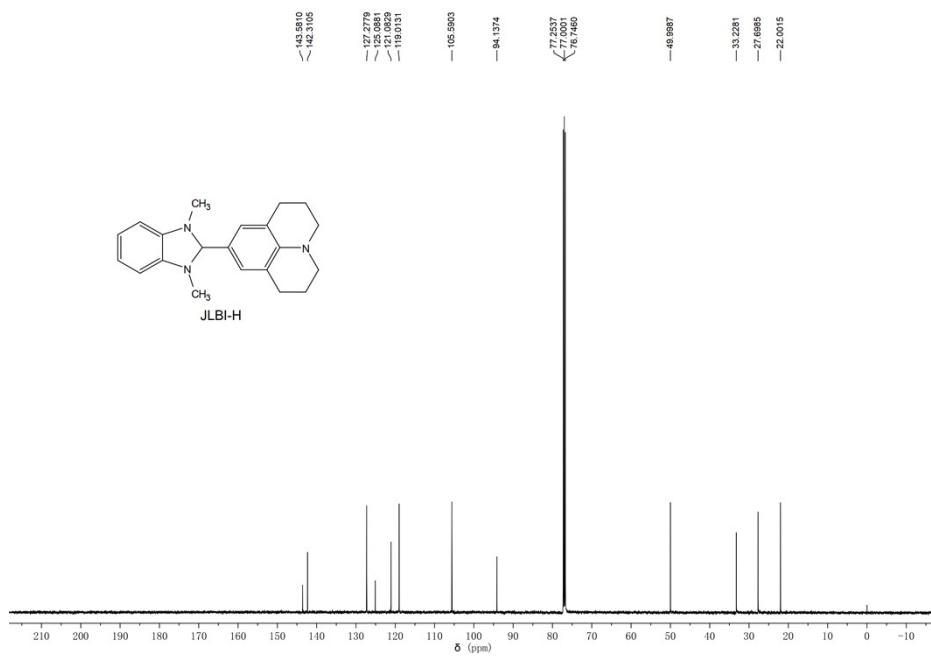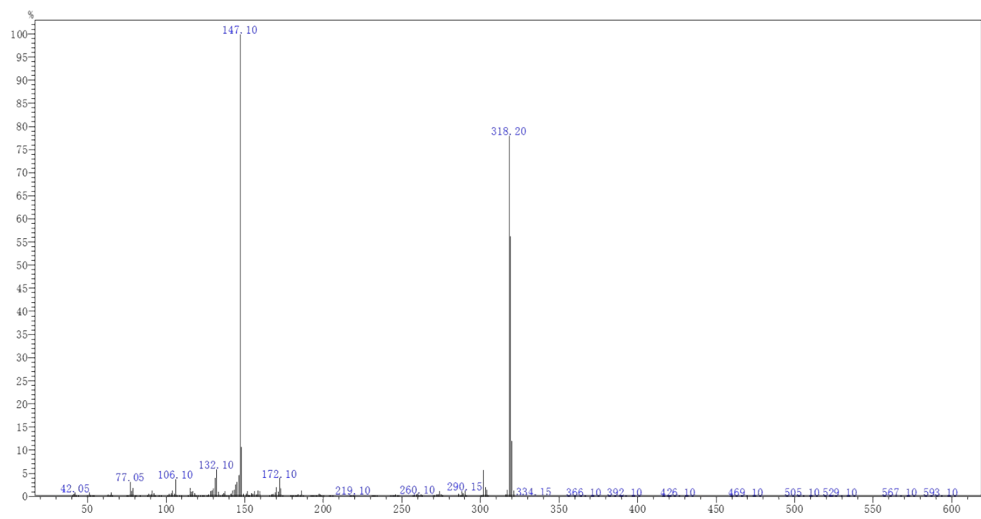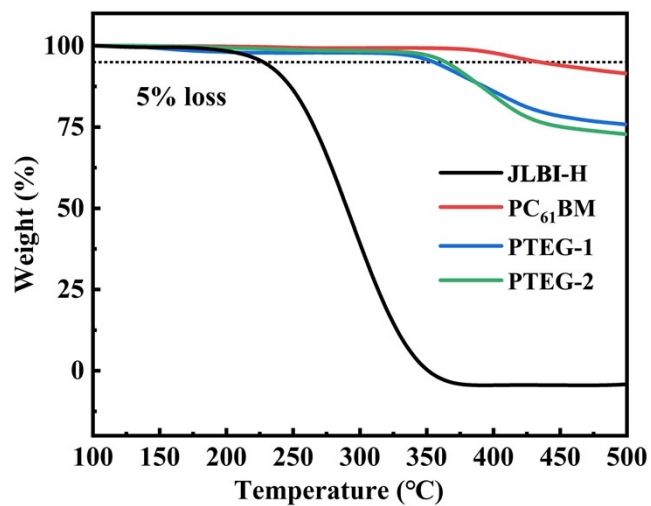

Fig. S1 The ^{1}H NMR spectrum of **JLBI-H** in CDCl$_3$.

Fig. S2 The ^{13}C NMR spectrum of **JLBI-H** in CDCl$_3$.

Fig. S3 The mass spectrometry of **JLBI-H**.

5. Figures of the Properties and Performances

Fig. S4 The TGA cures of **JLBI-H**, $PC_{61}BM$, PTEG-1, and PTEG-2 at a heating rate of 10
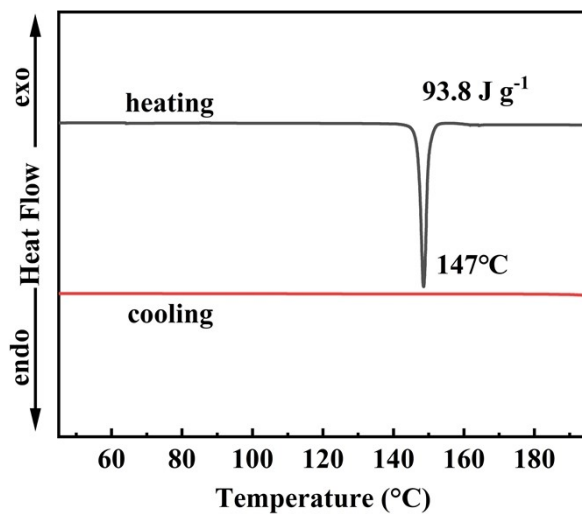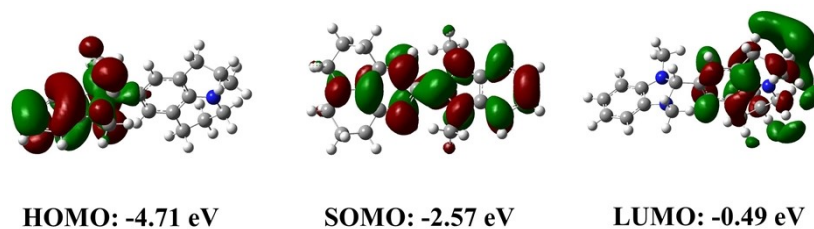
^oC min^{-1} under N_2.

Fig. S5 The DSC curve of **JLBI-H** from 30 to 200 ^oC under N_2 with a heating rate of 10
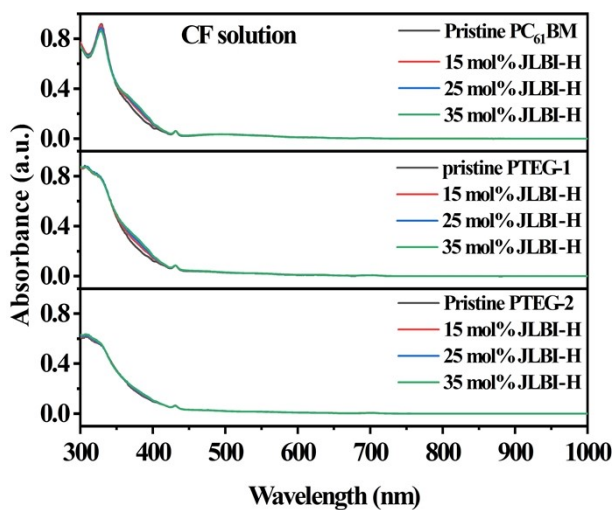
^oC min^{-1}.
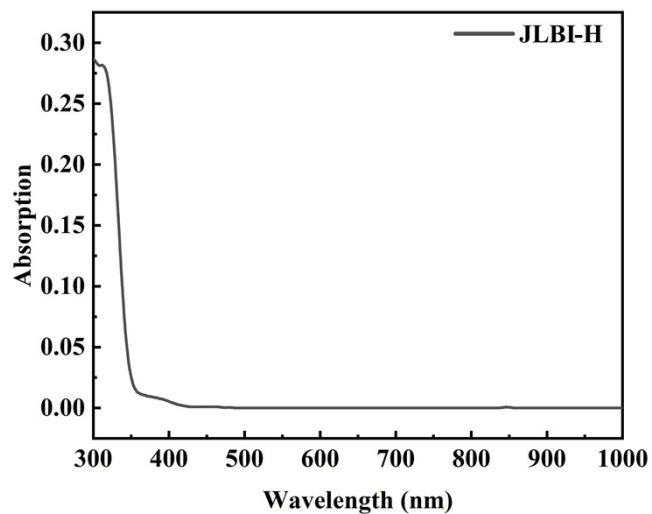
**Fig. S6** The UV-vis spectrum of **JLBI-H** solution in CH$_2$Cl$_2$ with the concentration of 1×10^{-5} M.
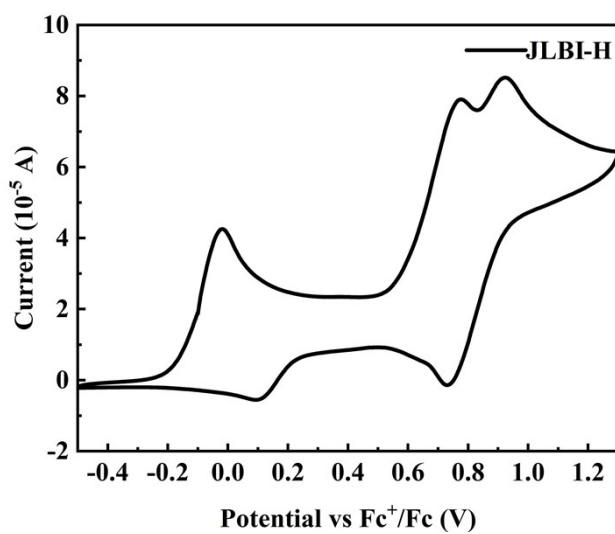
Fig. S7 The cyclic voltammetry curve of **JLBI-H** in deaerated anhydrous acetonitrile of 0.1 M Bu$_4$NPF$_6$ with a scan rate of 80 mV s^{-1}.

**HOMO: -4.71 eV**   **SOMO: -2.57 eV**   **LUMO: -0.49 eV**

Fig. S8 The pictorial representation and energies of the HOMO, LUMO of **JLBI-H** and the SOMO of **JLBI·**.

Fig. S9 UV-vis absorption spectra of pristine host, and blend solution of host and **JLBI-H** with various doping fractions. Fullerene derivatives concentrations of all the samples are 0.02 mg/ml (CF: chloroform).
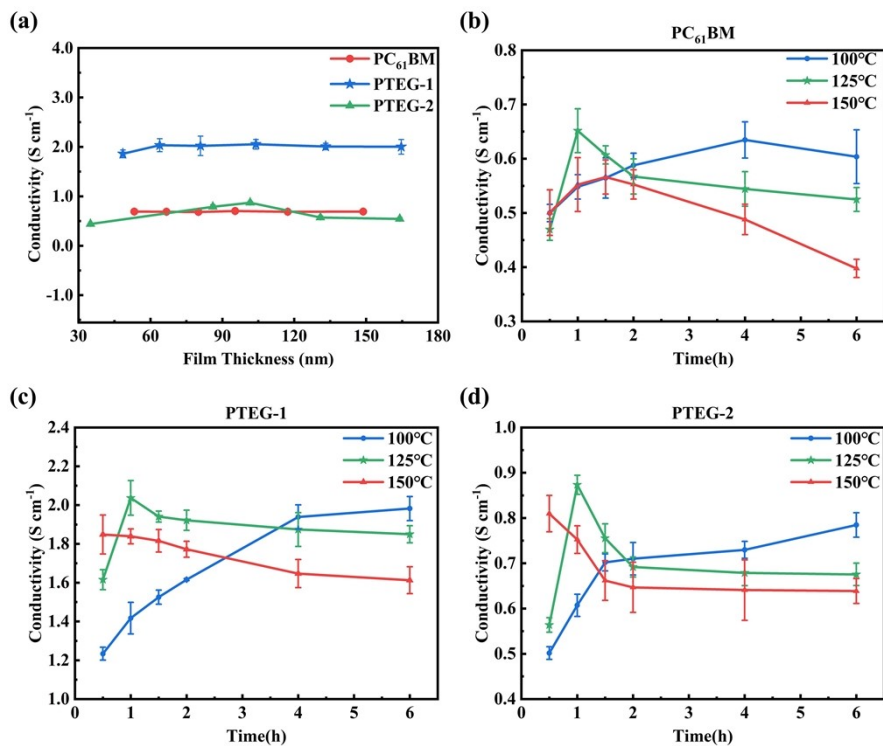
Fig. S10 The average electrical conductivity of the **JLBI-H** doped three fullerene films with various thickness (a) and the **JLBI-H** doped $PC_{61}BM$ (b), PTEG-1 (c), PTEG-2 (d) films annealed at various temperatures and durations. (The conductivity of each sample was obtained from at least 4 devices.)
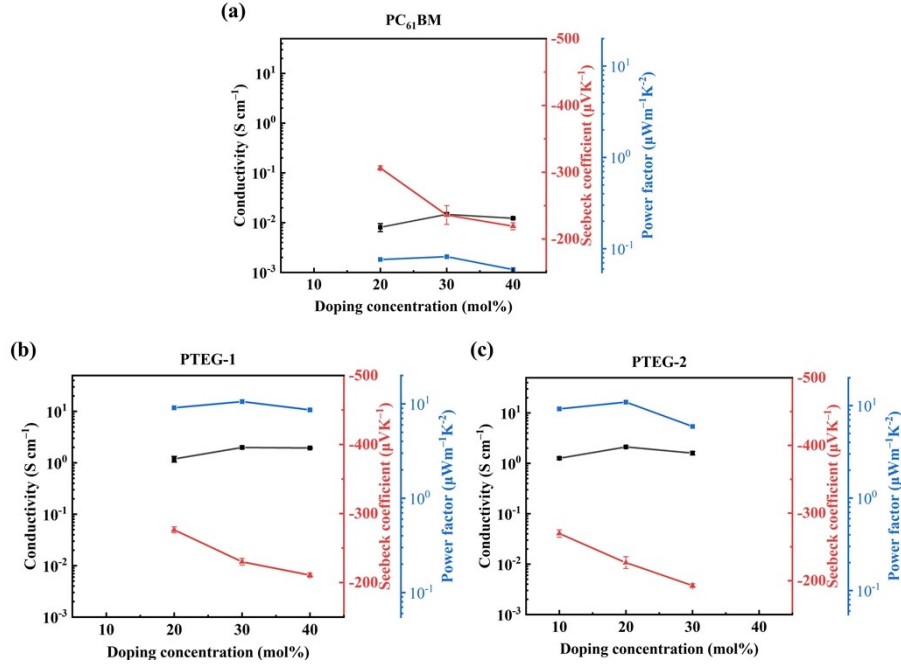
Fig. S11 Dependence of the electrical conductivity (σ), Seebeck coefficient (S) and power factor (PF) of the doped PC$_{61}$BM (a), PTEG-1 (b), PTEG-2 (c) films on the doping concentration of *N*-DMBI-H in molar fraction relative to the hosts.

Table S1 The PF_{max} as well as corresponding σ and S of *N*-DMBI-H doped PC$_{61}$BM、PTEG-1 and PTEG-2 films in this work and the previous literature.

Host	Annealing conditions	Doping fraction (mol%)	σ_{max} (S cm^{-1})	S (μV K^{-1})	PF_{max} (μW m^{-1} K^{-2})	Ref.
PC$_{61}$BM	125 ^{o}C, 1 h	30	1.4×10^{-2}	-235	8.0×10^{-2}	This work
	120 ^{o}C, 1.5 h	30	1.2×10^{-2}	-248	8.0×10^{-2}	(44)
PTEG-1	125 ^{o}C, 1 h	30	2.0	-230	10.6	This work
	120 ^{o}C, 1.5 h	40	2.0	-284	16.7	(44)
PTEG-2	125 ^{o}C, 1 h	20	2.1	-226	10.9	This work
	120 ^{o}C, 1 h	22	~2.0	~-230	~10.0	(41)[a]
	150 ^{o}C, 1 h	22	8.3	-230	41.0	(41)

[a] The values in this row were obtained from the thermoelectric parameter plots.

S16
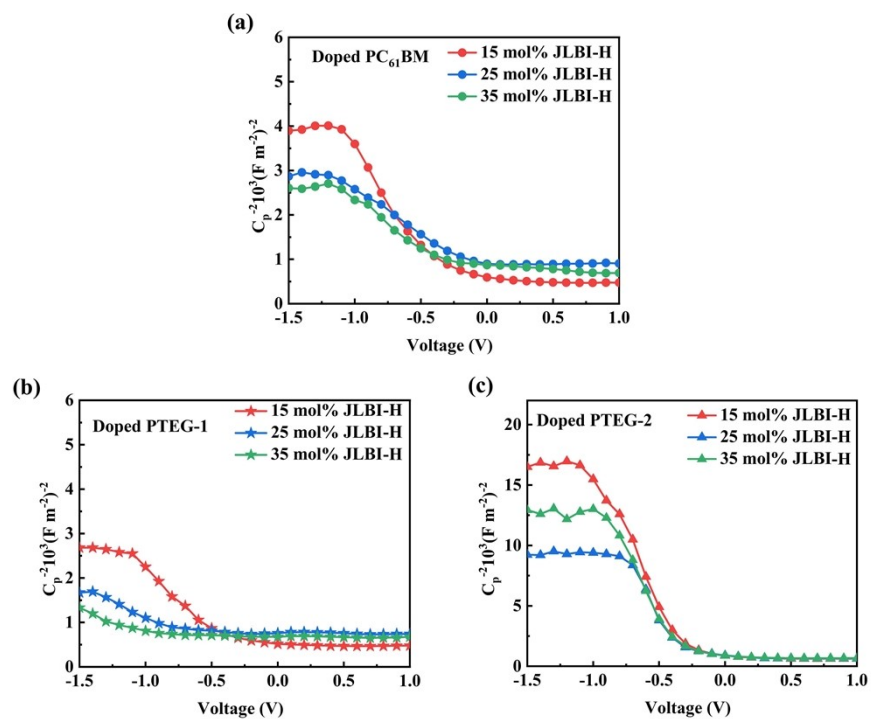
Fig. S12 Mott-Schottky plots for MIS devices based on $PC_{61}BM$ (a), PTEG-1 (b), PTEG-2 (c) films (annealed at 125 °C for 1 h) doped with various doping fractions of **JLBI-H**.
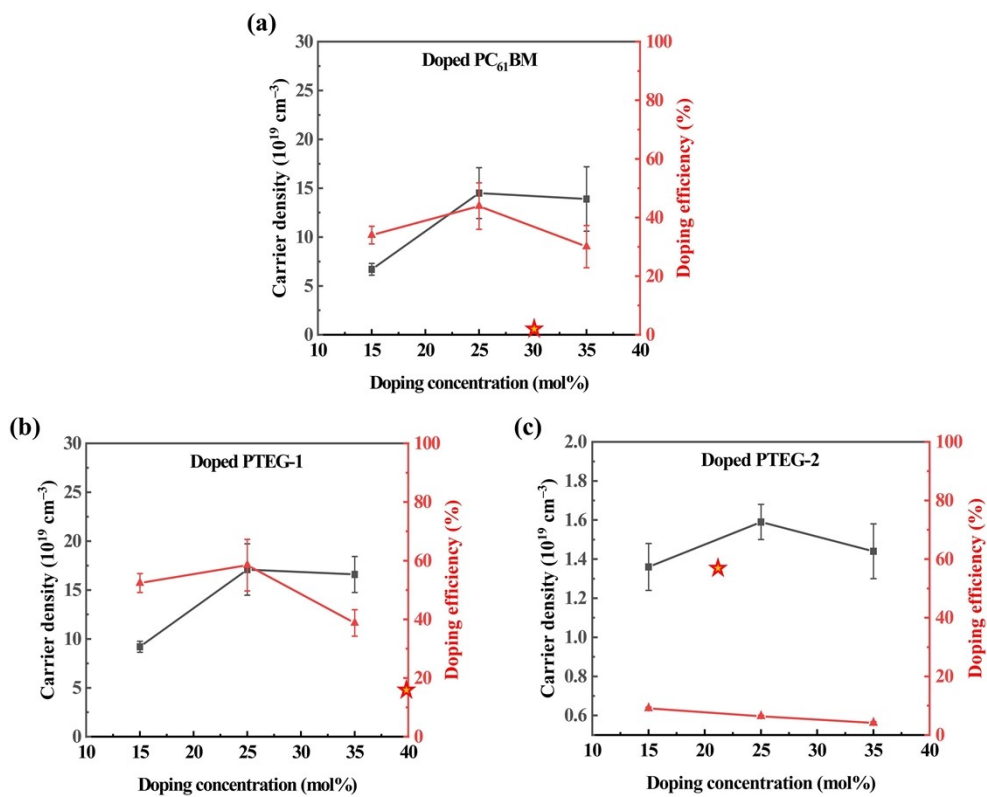
Fig. S13 Dependence of the carrier density and doping efficiency of doped $PC_{61}BM$ (a), PTEG-1 (b), PTEG-2 (c) films on the dopant fraction of **JLBI-H** in molar fraction relative to the hosts. The doping efficiencies of *N*-DMBI-H-doped fullerene derivatives from previous reports are also provided (★).
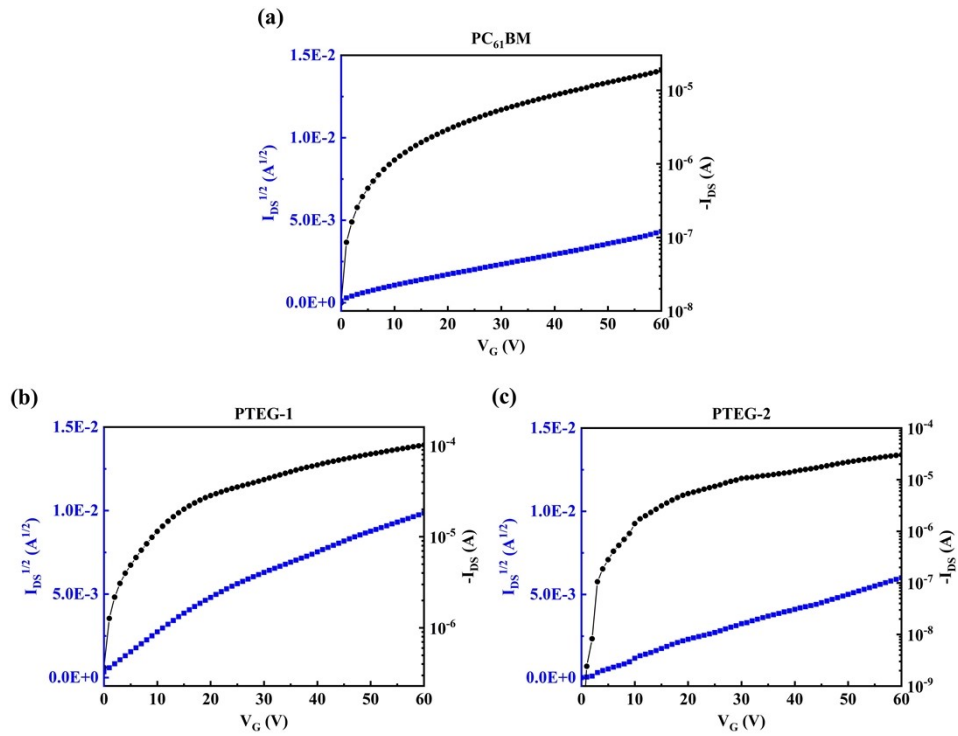
Fig. S14 Transfer characteristics of the OFETs devices with the 15 mol% **JLBI-H**-doped

PC$_{61}$BM (a), PTEG-1 (b) and PTEG-2 (c) active layers.
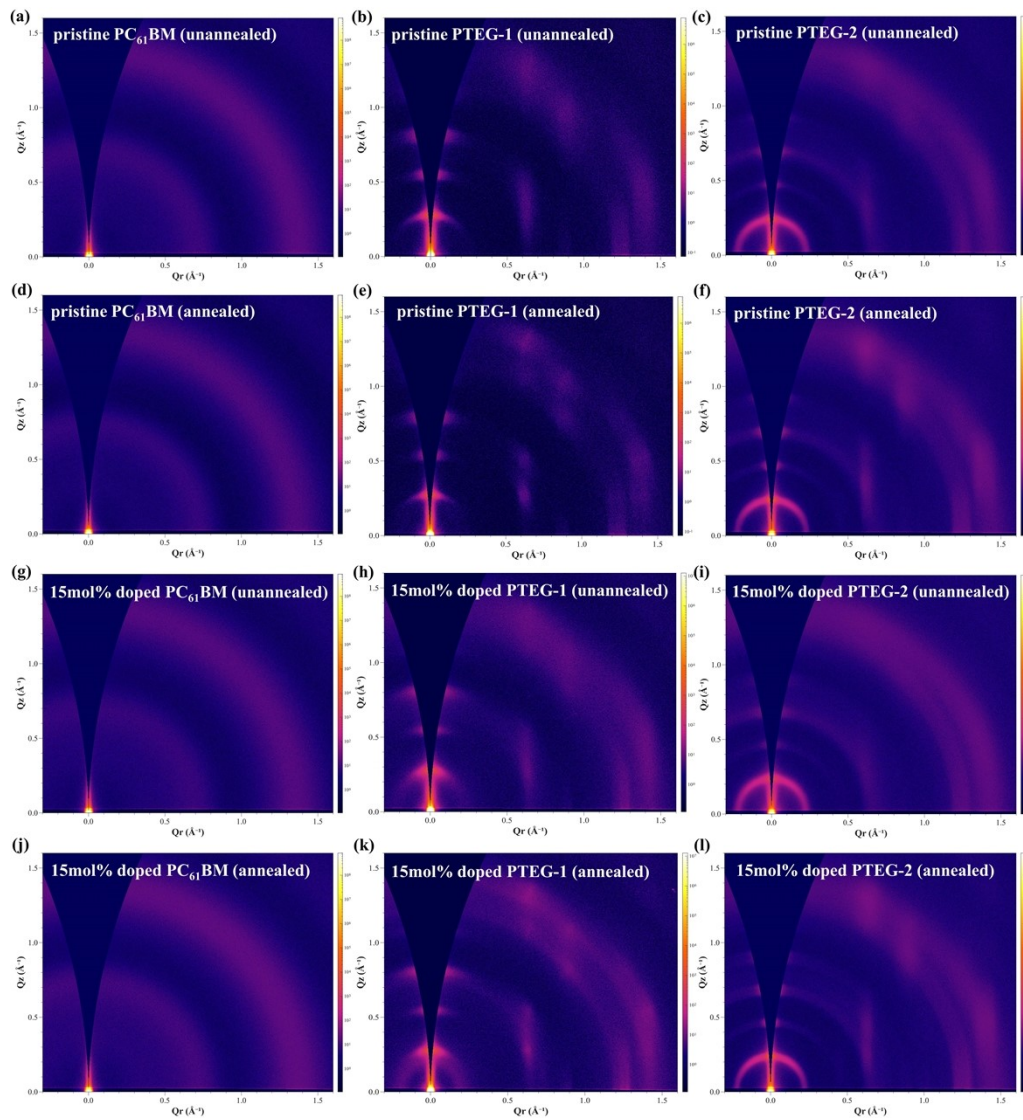
Fig. S15 GIWAXS patterns of the pristine fullerene films and the 15 mol% **JLBI-H** doped

$PC_{61}BM$, PTEG-1, PTEG-2 films before and after annealing at 125 °C for 1 h.
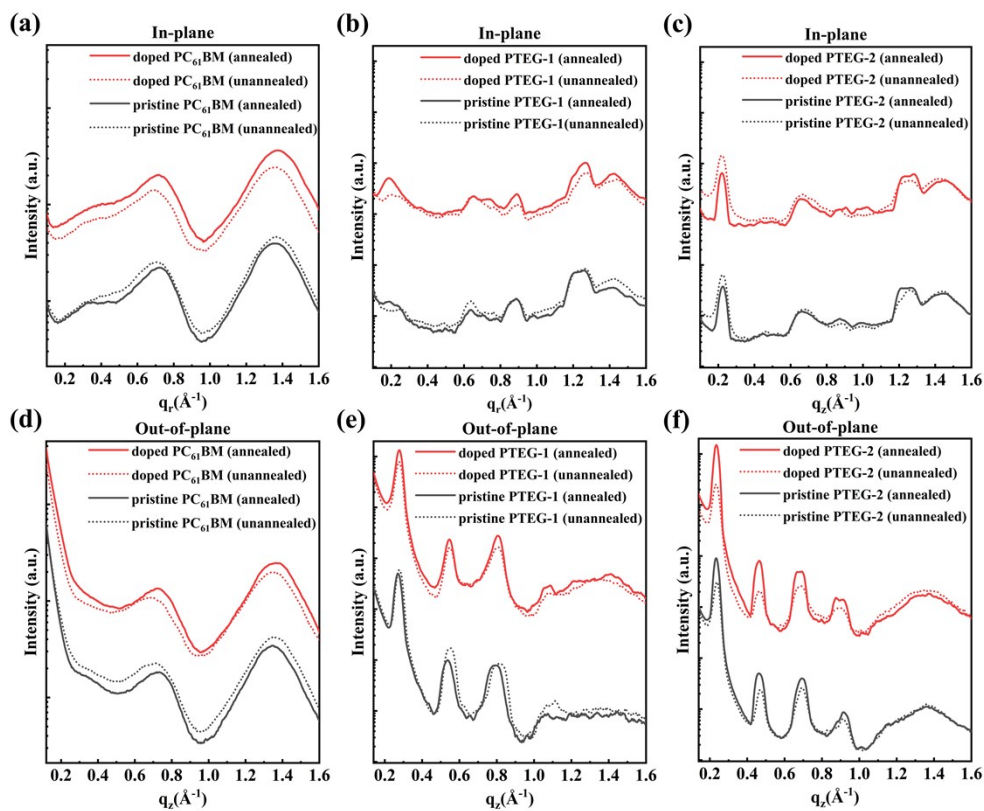
Fig. S16 GIWAXS scattering profiles along in-plane (IP, a,b and c) and out-of-plane (OOP, d,e and f) directions for the pristine fullerene films and the 15 mol% **JLBI-H**-doped $PC_{61}BM$, PTEG-1, PTEG-2 films before and after annealing at 125 ℃ for 1 h.
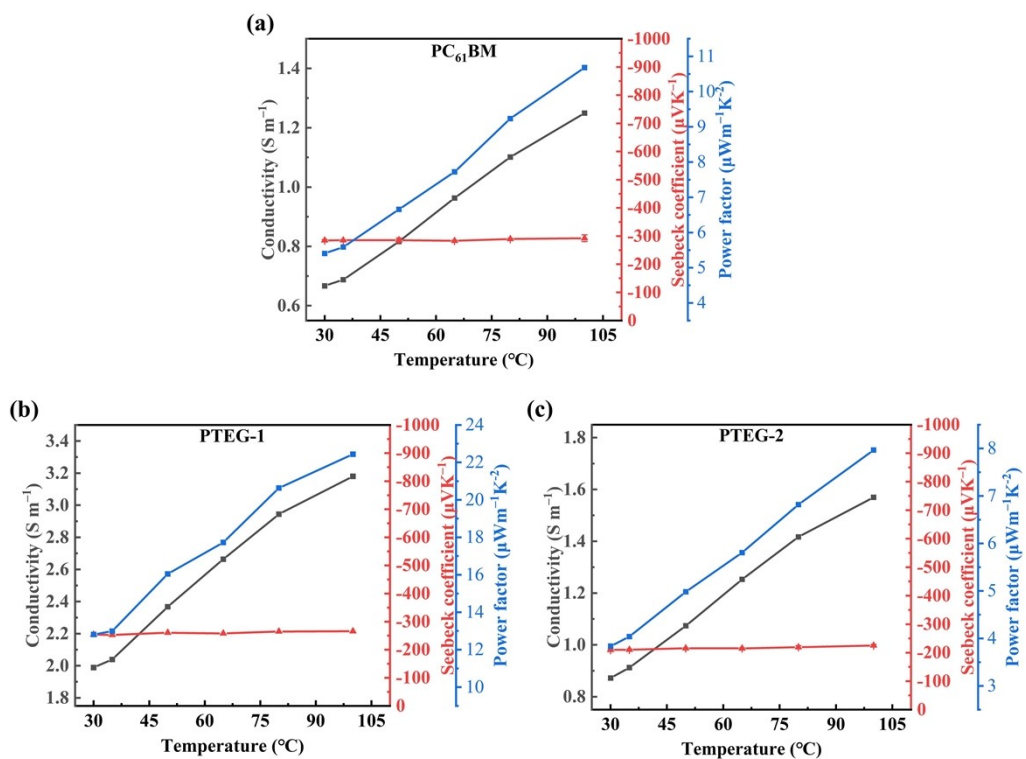
Fig. S17 Temperature-dependent conductivity and Seebeck coefficient of 15 mol% **JLBI-H**-doped $PC_{61}BM$ (a), PTEG-1 (b), and PTEG-2 (c) films after thermal annealing at 125 ℃ for 1h.
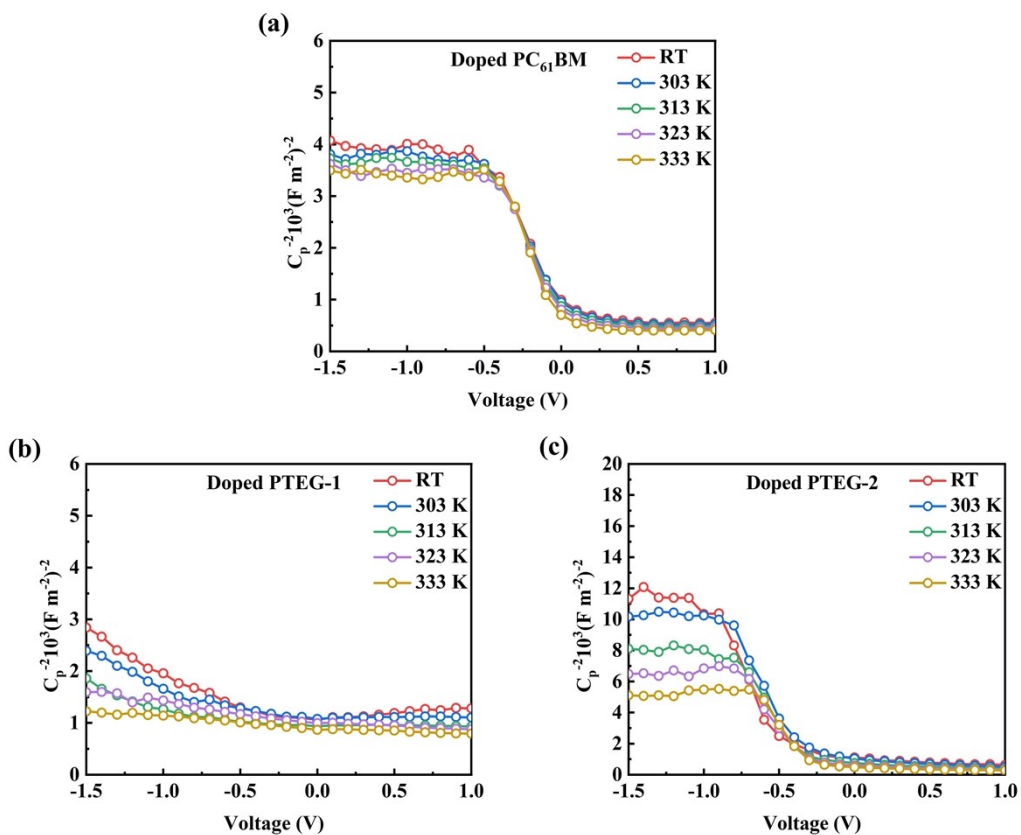
Fig. S18 Mott-Schottky plots for MIS devices based on 15 mol% **JLBI-H**-doped $PC_{61}BM$ (a), PTEG-1 (b), PTEG-2 (c) films (annealed at 125 °C for 1 h) at various temperature.

6. References

1. X. Q. Zhu, M. T. Zhang, A. Yu, C. H. Wang and J. P. Cheng, *J. Am. Chem. Soc.*, 2008, **130**, 2501-2516.

2. F. Jahani, S. Torabi, R. C. Chiechi, L. J. Koster and J. C. Hummelen, *Chem. Commun.*, 2014, **50**, 10645-10647.

3. M. J. Frisch, G. W. Trucks, H. B. Schlegel, G. E. Scuseria, M. A. Robb, J. R. Cheeseman, G. Scalmani, V. Barone, G. A. Petersson, H. Nakatsuji, X. Li, M. Caricato, A. V. Marenich, J. Bloino, B. G. Janesko, R. Gomperts, B. Mennucci, H. P. Hratchian, J. V. Ortiz, A. F. Izmaylov, J. L. Sonnenberg, Williams, F. Ding, F. Lipparini, F. Egidi, J. Goings, B. Peng, A. Petrone, T. Henderson, D. Ranasinghe, V. G. Zakrzewski, J. Gao, N. Rega, G. Zheng, W. Liang, M. Hada, M. Ehara, K. Toyota, R. Fukuda, J. Hasegawa, M. Ishida, T. Nakajima, Y. Honda, O. Kitao, H. Nakai, T. Vreven, K. Throssell, J. A. Montgomery Jr., J. E. Peralta, F. Ogliaro, M. J. Bearpark, J. J. Heyd, E. N. Brothers, K. N. Kudin, V. N. Staroverov, T. A. Keith, R. Kobayashi, J. Normand, K. Raghavachari, A. P. Rendell, J. C. Burant, S. S. Iyengar, J. Tomasi, M. Cossi, J. M. Millam, M. Klene, C. Adamo, R. Cammi, J. W. Ochterski, R. L. Martin, K. Morokuma, O. Farkas, J. B. Foresman and D. J. Fox, 2016.

4. S. Riera-Galindo, A. Orbelli Biroli, A. Forni, Y. Puttisong, F. Tessore, M. Pizzotti, E.

Pavlopoulou, E. Solano, S. Wang, G. Wang, T. P. Ruoko, W. M. Chen, M. Kemerink, M. Berggren, G. di Carlo and S. Fabiano, *ACS Appl. Mater. Interfaces.*, 2019, **11**, 37981-37990.